PERGAMON

Electrochimica Acta 47 (2002) 3853–3861

ELECTROCHIMICA Acta

www.elsevier.com/locate/electacta

Lithium/V_6O_{13} cells using silica nanoparticle-based composite electrolyte

Yangxing Li, Peter S. Fedkiw *, Saad A. Khan

Department of Chemical Engineering, North Carolina State University, P.O. Box 7095, 107 Riddick Hall, Raleigh, NC 27695-7905, USA

Received 4 March 2002; received in revised form 17 May 2002

Abstract

The electrochemical behavior of Li/V_6O_{13} cells is investigated at room temperature (22 °C) both in liquid electrolyte consisting of oligomeric poly(ethyleneglycol)dimethylether+lithium bis(trifluoromethylsulfonylimide) and composite electrolytes formed by blending the liquid electrolyte with silica nanoparticles (fumed silica). The addition of fumed silica yields a gel-like electrolyte that demonstrates the desirable property of suppressing lithium dendrite growth due to the rigidity and immobility of the electrolyte structure. The lithium/electrolyte interfacial resistance for composite gel electrolytes is less than that for the corresponding base-liquid electrolyte, and the charge–discharge cycle performance and electrochemical efficiency for the Li/V_6O_{13} cell is significantly improved. The effect of fumed silica surface group on the electrochemical performance is discussed; the native hydrophilic silanol surface group appears better than fumed silica that is modified with a hydrophobic octyl surface moiety.

Keywords: Lithium cell; Composite gel electrolyte; Silica nanoparticle; Lithium dendrite; Vanadium oxide

1. Introduction

The use of gel polymer electrolytes has opened a new avenue in the field of polymer electrolytes due to their improved performance compared with conventional electrolytes. Of interest here is a class of gel electrolytes that have the dual merits [1–5] of a liquid possessing high conductivity at room temperature (10^{-3} S cm^{-1}) and a solid with good mechanical strength that can minimize or eliminate electrolyte leakage. Gel electrolytes, which were originally introduced by Feuillade and Perche in 1975 [6], can be classified into physical cross-linked and chemical cross-linked structures [7]. Gel electrolytes have received attention owing to their proposed application in rechargeable lithium batteries and electrochemical supercapacitors [8].

Even though the commercial application of lithium-ion batteries has succeeded in many aspects, lithium batteries remain attractive since metallic lithium has a more negative potential and a high-specific capacity of 3800 mA h g^{-1}. However, the use of a lithium anode for rechargeable batteries presently has significant disadvantages such as deleterious dendrite formation, low-cycle efficiency, and safety concerns [9]. Because the electrolyte plays a major role in these issues, finding a suitable electrolyte is key for the commercialization of rechargeable lithium metal batteries.

Typically, gel-type electrolytes contain lithium salt and non-aqueous solvent dispersed in an inert polymer matrix. The polymer matrix provides mechanical strength and may be chosen from a variety of polymers [7], including polyacrylonitrile, poly(methylmethacrylate), poly(vinylchloride), poly(vinylsulfone), poly(vinylidenefluoride), among others. In contrast, our unique composite gel electrolytes are based on fumed silicas that are an amorphous, nonporous type of silica (SiO_2) with branched-aggregate structures containing a primary particle size about 12 nm [10]. The native surface group on fumed silica is silanol (Si–OH), which can be replaced by other moieties such as alkyls or alkyl methacrylates, among others. Gel polymer electrolytes are obtained by dispersing fumed silica particulates into a liquid electrolyte that is composed of low-molecular

* Corresponding author. Tel.: +1-919-515-3572; fax: +1-919-515-3465

E-mail address: fedkiw@eos.ncsu.edu (P.S. Fedkiw).

0013-4686/02/$ - see front matter
PII: S0013-4686(02)00326-2

poly(ethyleneglycol)dimethylether+lithium salt. These composites exhibit desirable mechanical properties characteristic of solids (elastic modulus G′ in excess of 10^5 Pa), yet have the processability of liquids and display conductivities rivaling liquid electrolytes ($\approx 10^{-3}$ S cm^{-1} at 25 °C) [1–3]. These characteristics are a direct consequence of the self-assembly of the fumed silica to form three-dimensional continuous networks originating from hydrophobic interactions, solvation forces and/or hydrogen bonding of the surface groups on the silica [11,12]. In this paper, we focus on the effects of fumed silicas with different surface groups on the electrochemical behavior of the Li/V_6O_{13} cell, which is a candidate for use in electric vehicles [13].

2. Experimental

2.1. Electrolyte preparation

Lithium bis(trifluoromethylsulfonylimide) ($LiN(CF_3SO_2)_2$, LiTFSI, 3 M) was dried in a vacuum oven ($\sim 10^{-4}$ Torr) at 100 °C to constant weight. Fumed silicas (Aerosil A200 and R805, Degussa) were also dried in a vacuum oven at 120 °C for about a week. The R805 fumed silica contains octyl surface group at 48% coverage and silanol surface group at 52% coverage, and the A200 fumed silica contains only native silanol on the surface [12]. Poly(ethyleneglycol)dimethylether ($CH_3O–(CH_2–CH_2–O–)_nCH_3$, PEGdm, Mw 250, Aldrich) was dried over 4 Å molecular sieves for at least 1 week before use. The liquid electrolyte was made by dissolving LiTFSI into the PEGdm with a mole ratio 1:20 (Li:O) to reach the highest conductivity [1]. Sample preparation and cell assembly were carried out in an Argon-filled glove box. The composite gel electrolytes were prepared by dispersing 10 wt.% fumed silica A200 or R805 into the liquid electrolyte using a high-shear mixer (Tissue-Tearor, BioSpec Products). The mixtures were centrifuged (IEC HN-SII centrifuge, Damon/IEC Division) in order to remove gas bubbles but without disrupting the gel network. The water content of the composite electrolytes was less than 50 ppm, as determined by Karl–Fisher titration.

2.2. Electrode preparation

Composite electrodes were prepared by tumble-mixing the active material V_6O_{13} (Kerr–McGee)+graphite (Timcal American)+Ketjen-Black600 (Akzo Nobel)+poly(vinylidenedifluoride) (KYNAR) with the mass ratio 75:10:5:10, respectively. The mixtures were dispersed in 1-methyl-2-pyrrolidinone (NMP, Aldrich) and tumble-mixed for about 12 h. The resulting slurry consisting of 30% solids was cast onto an Al foil current collector with a doctor blade to control the thickness at 102 μm. The film was dried in an oven at 80 °C for 24 h, then was punched into half-inch (1.27 cm) diameter disks which were hot-compacted in a hydraulic press (Carver) at 150 °C under about 34 MPa. After compaction, the cathode electrode was dried in a vacuum oven at 150 °C for at least 24 h before use.

2.3. Cell assembly and testing

Coin cells in which an electrolyte/separator was sandwiched between two electrodes were assembled in an Argon-filled glove box. The separator is Celgard 2400 that was wetted by the liquid electrolyte, or for the composite electrolytes, the Celgard film was sandwiched between two layers of the composite gel; alternatively, the separator is a 500 μm thick polypropylene (PP) mesh that was sandwiched between two layers of composite gel electrolyte. The mesh has an open-area fraction of 47% and a 'pore size' of approximate 200 μm. Lithium metal (Aldrich) was punched into a half-inch disc (1.27 cm) as an anode electrode. 'Half cells' (Li/electrolyte/Li) and full cells ($Li/electrolyte/V_6O_{13}$) were made to evaluate the interfacial stability and cycle performance, respectively. Different currents were applied in the cell cycling using an Arbin battery cycler (Model BT2042) controlled by ARBIN ABTS software. Li/electrolyte/Li cells were cycled at current densities of 0.2 mA cm^{-2} with a charge density of 1.44 C cm^{-2}. Full cells were cycled at C/15 with a voltage window between 1.8 and 3.0 V. Impedance measurements were carried out using a Zahner IM6e impedance analyzer. The open-circuit potential impedance spectra were normally recorded in a frequency range of 100 kHz–0.1 Hz with an oscillation amplitude of 10 mV. All measurements were taken at room temperature, approximately 22 °C.

3. Results and discussion

3.1. Li/Li cycle

In cycling a Li/Li cell, a lithium electrode alternatively acts as the source (anode) and sink (cathode) of lithium, and a passive layer is continuously formed and disrupted at its surface [9]. The Li/Li cycling test was performed by passing a constant current of 0.2 mA cm^{-2} through the cell and reversing the current polarity every 2 h (1.44 C cm^{-2}). Fig. 1 shows typical results with different electrolytes: (a) liquid electrolyte; (b) composite electrolyte using 10% A200 (silanol terminated hydrophilic fumed silica); and, (c) composite electrolyte using 10% R805 (octyl-modified hydrophobic fumed silica). The cell voltage using composite electrolytes, whether A200 or R805, is more stable than that with liquid electrolyte. The oscillation of cell voltage with the liquid electrolyte indicates lithium dendrite

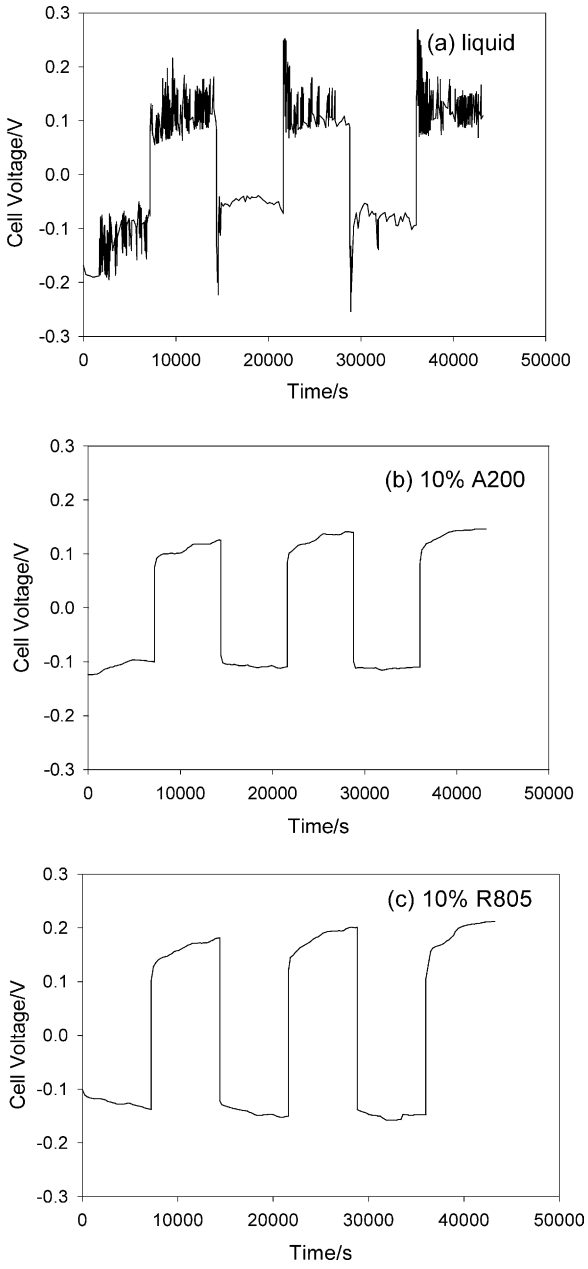

Fig. 1. Typical cell voltage behavior of Li/Li cells cycling at 0.2 mA cm^{-2} for 2 h: (a) liquid electrolyte; (b) 10% A200 (silanol-terminated hydrophilic fumed silica) gel; (c) 10% R805 (octyl-modified hydrophobic fumed silica) gel.

growth even in the first cycle [14,15]. The extent of growth during cycling depends on the current and time, with high current and long time facilitating growth. In Fig. 1(a), we see that the cell voltage varies smoothly until 1.68×10^3 s in the first cycle; that is, after passing 0.336 C cm^{-2} dendrite formation began using the liquid electrolyte. Lithium dendrite growth, a common phenomenon for liquid electrolytes, is undesirable since it results in electronically isolated lithium upon cycling, which lowers the coulombic efficiency. Also, dendrites are unsafe and may induce an internal short circuit. From Fig. 1(b) and (c), it is evident that the composite gel electrolyte inhibits lithium dendrite formation, as reported by others [16–18]. One possible reason is that the gel mechanically inhibits dendrite formation and growth due to the rigidity and immobility of the gel electrolyte. During the first three cycles, the maximum cell voltages for the different electrolytes are 0.269, 0.146, and 0.212 V corresponding, respectively, to liquid electrolyte, 10% A200 composite, and 10% R805 composite. The improvement effect of fumed silicas seen in these Li/Li cells is congruent with the full-cell cycling data reported in the next section.

Fig. 2 reports the impedance spectra of Li/Li cells after 20 cycles. All three electrolytes exhibit a depressed semicircle and a line at low frequency inclined at about 35 ° to the real axis. The sequence of interfacial resistances (Table 1), determined by the method of Fauteux [19], is R_{int}(10% A200) < R_{int}(10% R805) < R_{int}(liquid electrolyte). These results are consistent with the voltage behavior in the Li/Li cycling.

We also investigated the cycling of Li/Li cells using an open-mesh polypropylene screen to separate the two lithium electrodes to exclude any possible effect of the Celgard membrane and better control interelectrode spacing. We evaluated the cycle performance using A200- or R805-based composite electrolytes; liquid electrolyte could not be used since it was not held within the large voids in the screen. The open-area fraction of the mesh is 47%, and we calculate the current density based on the total electrode area. The lithium stripping/plating current density was 0.2 mA cm^{-2} for 2 h at 22 °C, which are the same conditions used with Celgard. The voltage behavior of the first 20 cycles is shown in the Fig. 3, and the results are similar to those in Fig. 1 using Celgard. Both composite electrolytes show similar characteristics; the average cell voltage rises over the first several cycles and then decreases, and an oscillatory behavior appears in the following cycles, presumably due to lithium dendrite formation. After the

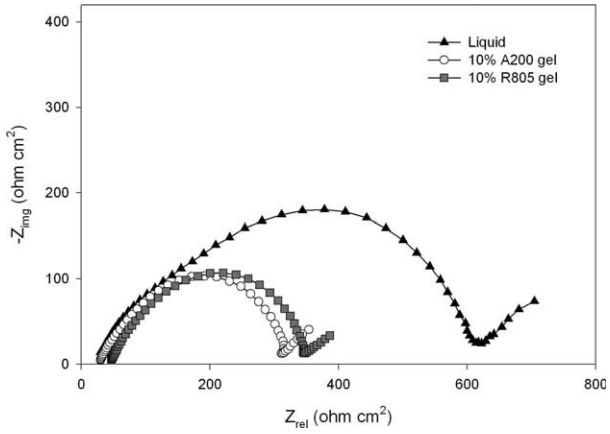

Fig. 2. Impedance spectra of Li/Li cells after 20 cycles with three different electrolytes, cycle conditions as in Fig. 1.

Table 1
Resistances of Li/Li cells with different electrolytes after 20 cycles

Electrolytes	R_{bulk} (Ω cm^2)	R_{int} (Ω cm^2)
Liquid electrolyte	12.8	545
10% A200 gel	32.5	267
10% R805 gel	43.5	279

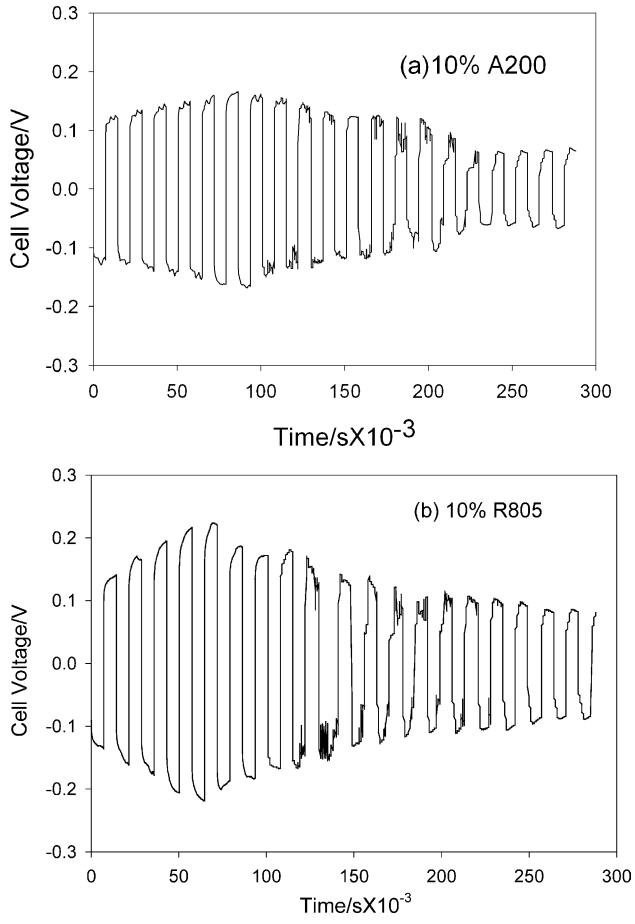

Fig. 3. Cycle performance of Li/Li cells with polypropylene mesh as separator at 0.2 mA cm^{-2} for 2 h in each direction: (a) 10% A200 gel; (b) 10% R805 gel.

interface becomes stable, the cell voltage does not fluctuate. The cell voltage for 10% R805 is greater than that for 10% A200 composite electrolyte, the same trend seen with Celgard 2400.

3.2. Li/V_6O_{13} cycle

Full-cell Li/electrolyte/V_6O_{13} cycling performance was evaluated at room temperature (22 °C). The cycling is initiated by a discharge first to 1.8 V followed by a charge to 3.0 V. The electrode reactions during charge and discharge are

$$\text{Cathode} \quad V_6O_{13} + xLi^+ + xe^- \underset{\text{charge}}{\overset{\text{discharge}}{\rightleftharpoons}} Li_xV_6O_{13} \qquad (1)$$

$$\text{Anode} \quad xLi \underset{\text{charge}}{\overset{\text{discharge}}{\rightleftharpoons}} xLi^+ + xe^- \qquad (2)$$

Theoretically, the maximum lithium uptake is 8 mol Li per formula unit for a capacity of 417 mA h g^{-1} [20], which is the value used in our determination of C rate. The number of 'electronic sites' rather than ionic sites limits lithium uptake since the mean oxidation number of vanadium is about 3 [21].

Typical charge–discharge curves for Li/CPE/V_6O_{13} are shown in Fig. 4 when cycling at 0.158 mA cm^{-2}

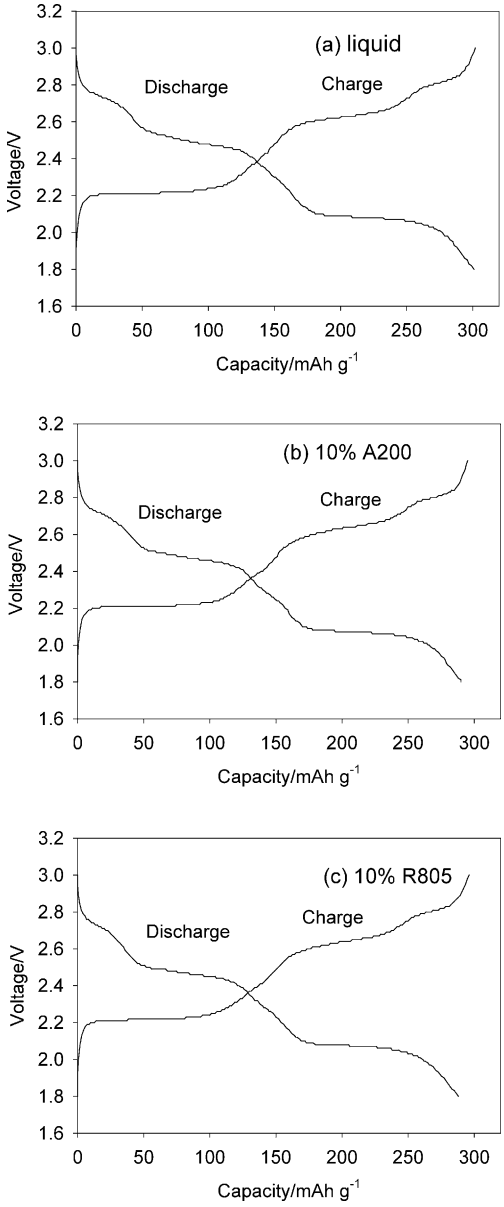

Fig. 4. Typical (third) charge–discharge curves for Li/V_6O_{13} cells: (a) liquid electrolyte; (b) 10% A200 gel; (c) 10% R805 gel. The cycle conditions are C/15 current (0.158 mA cm^{-2}), voltage range 1.8–3.0 V, and room temperature (22 °C).

between 1.8 and 3.0 V (C/15 current rate, 27.2 mA g^{-1}). The data are for the third charge/discharge cycle using three different electrolytes: (a) liquid; (b) 10% A200; and (c) 10% R805. The initial discharge capacities are all about 300 mA h g^{-1}, corresponding to 5.75 mol Li intercalated per mol V_6O_{13}. The charge curves show three distinct voltage plateaus (about 2.2, 2.6, and 2.8 V); the discharge curves also show three distinct plateaus (about 2.1, 2.5, and 2.7 V), except these voltages are lower than those in the corresponding charge process. The capacity ratio at the three voltage plateaus (charge or discharge) is approximately 1:2:4 in the sequence of high:intermediate:low voltage. These phenomena are also observed in the electrochemical voltage spectroscopy (EVS), a technique originally devised by Thompson [22]. Fig. 5 shows the EVS profiles calculated from the data in Fig. 4, and all have three distinct charge and discharge peaks. The

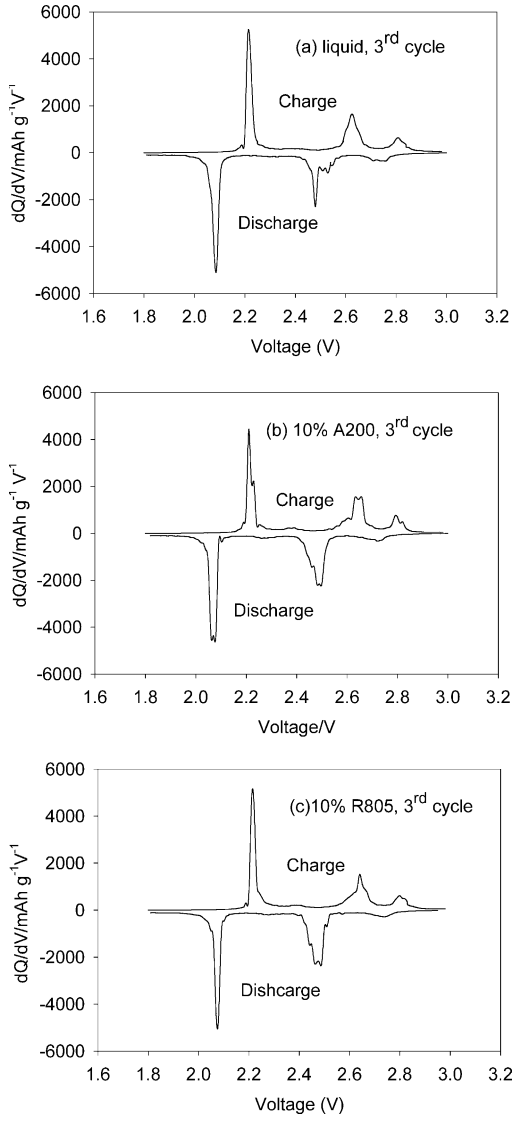

Fig. 5. EVS profiles of Li/V_6O_{13} cells, derived from Fig. 4.

results show that, at the low current density used, the choice of electrolyte does not affect the voltage-capacity behavior of the fresh V_6O_{13} electrodes. Although the charge/discharge profiles are similar, the EVS curves show slight differences that are due to the varied electrolyte/electrode interfaces between the cells although numerical artifacts and cell-to-cell variability should be considered.

The initial performance is similar for all cells, but capacity retention is improved with electrolytes containing fumed silica. Fig. 6 reports the cycle performance for Li/V_6O_{13} cells with different electrolytes cycled at C/15 in the voltage range of 1.8–3.0 V at 22 °C. The initial capacities in different electrolytes are all comparable at about 300 mA h g^{-1}, or 5.75 mol Li per mol V_6O_{13}, which is a high-discharge capacity. Although capacity fading is present in all electrolytes, the composite electrolytes show better performance: the capacities of cells containing 10% A200 and 10% R805 electrolyte are about two times that of the liquid electrolyte after 20 cycles. The different surface groups on the fumed silicas affect the cycling performance: A200 appears better than R805 with the 20th cycle specific capacity about 211 and 203 mA h g^{-1}, respectively. Capacity fading during cycling is a common phenomenon in solid-state cells and may be ascribed to a number of factors: irreversible structural changes for these intercalation materials; contact loss between the electronic conductive material and the redox active materials in the composite electrodes; and, depletion of electrolytes due to reaction [23]. According to the literature, V_6O_{13} undergoes an irreversible structural change. The unit cell dimensions for uncycled V_6O_{13} ($a = 11.821$, $b = 3.685$, $c = 10.098$ Å, and $\beta = 100.81°$) differs from those for cycled, essentially lithium-free V_6O_{13} ($a = 11.87$, $b = 3.716$, $c = 10.25$ Å, and $\beta = 101.01°$) [24]. Also, the vanadium oxide molar volume rises about 9% upon intercalating 5.75

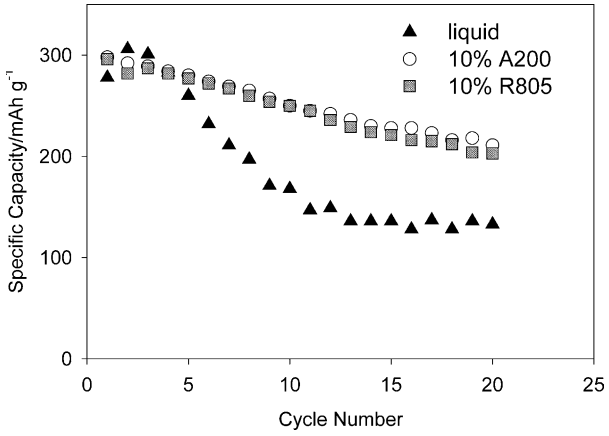

Fig. 6. Cycling behavior for Li/V_6O_{13} cells with different electrolytes. Charge–discharge at C/15 rate (0.158 mA cm^{-2}); voltage range of 1.8–3.0 V; cathode material loading of 5.8 mg cm^{-2}; temperature 22 °C.

mol Li per mol V_6O_{13} [20]. The repeated expansion/contraction during cell cycling induces a loss of contact between the cathode particles and the conductive material.

To investigate further the capacity-fade phenomenon, we report the charge–discharge voltage profiles and EVS at the 10th and 20th cycle. Fig. 7 shows the discharge–charge profiles, and Fig. 8 reports the corresponding EVS. The capacity at all three voltage plateaus decreased during cycling, both in charge and discharge. However, the charge/discharge curves of the composite electrolytes more closely follow their first-cycle shape than those of liquid electrolyte. During the first 20 cycles, the charge capacity at 2.2 V with a liquid electrolyte decreases significantly, and at the 20th cycle it is even less than that at 2.6 V; in contrast to the charge profiles, the ratio of discharge capacity at the three voltage plateaus is nearly the same at 20th cycle as that at third cycle (Fig. 4). One possible reason for the different capacity fading at different voltages is the varying electronic conductivity and diffusion coefficient [21] of lithium in lithitated vanadium oxides. During charge, the electronic conductivity and the diffusion coefficient of lithium is less at the lowest voltage stage (about 2.2 V), which we anticipate is a factor in the pronounced capacity decrease at the lowest voltage plateau upon cycling.

The average charge–discharge voltage at each cycle is illustrated in Fig. 9 for the three different electrolytes.

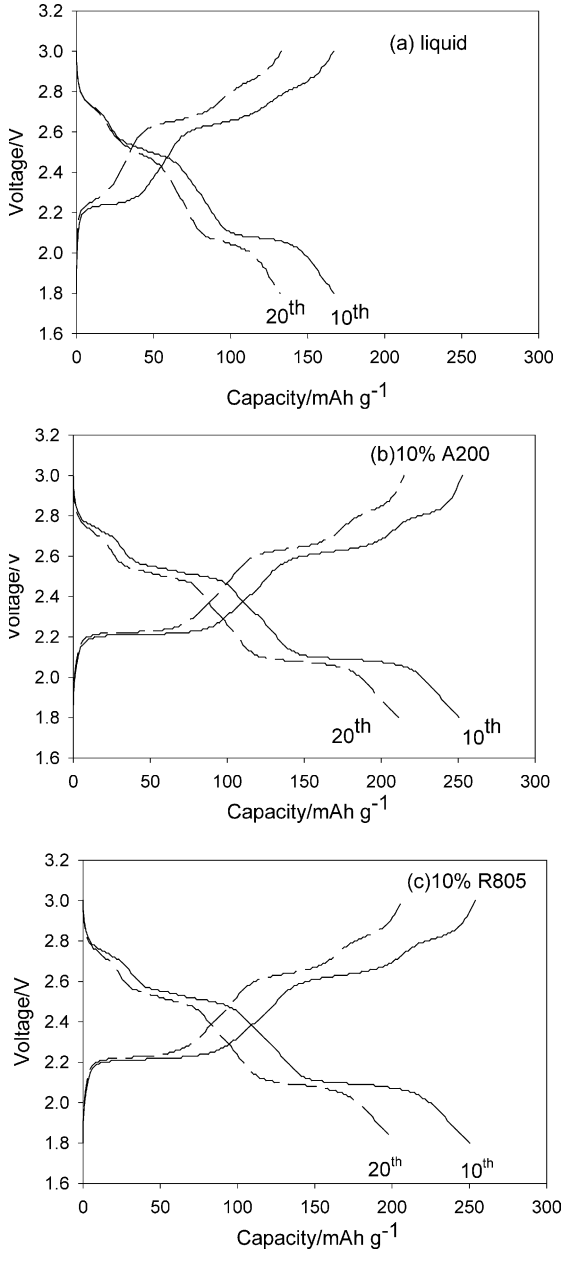

Fig. 7. Charge–discharge curves for Li/V_6O_{13} cells with different electrolytes at different cycles: (a) liquid electrolyte; (b) 10% A200 gel; (c) 10% R805 gel. The cycle conditions are the same as in Fig. 4.

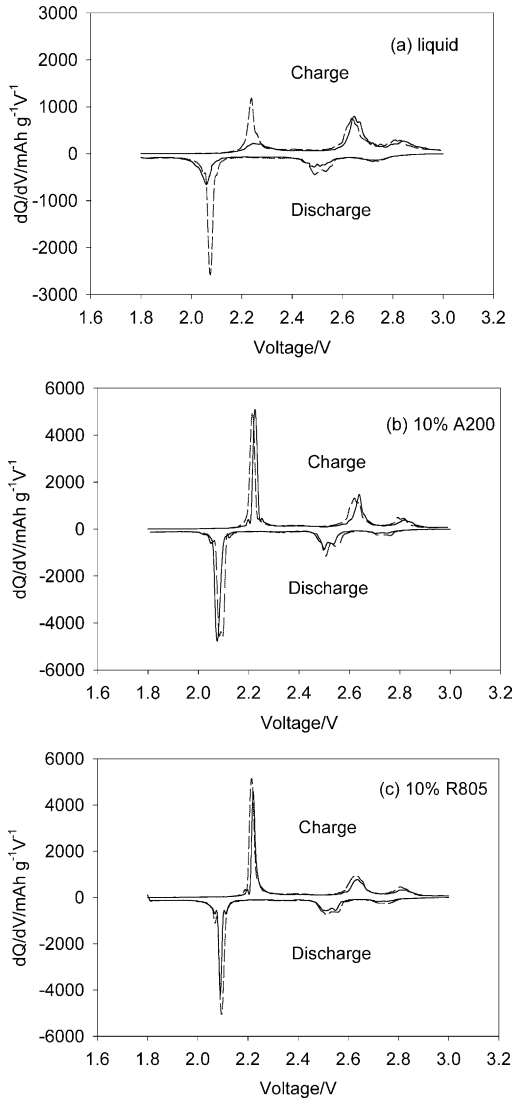

Fig. 8. EVS curves of Li/V_6O_{13} cells at 10th and 20th cycle with different electrolytes, derived from Fig. 7 (dashed line: 10th cycle; solid line: 20th cycle).

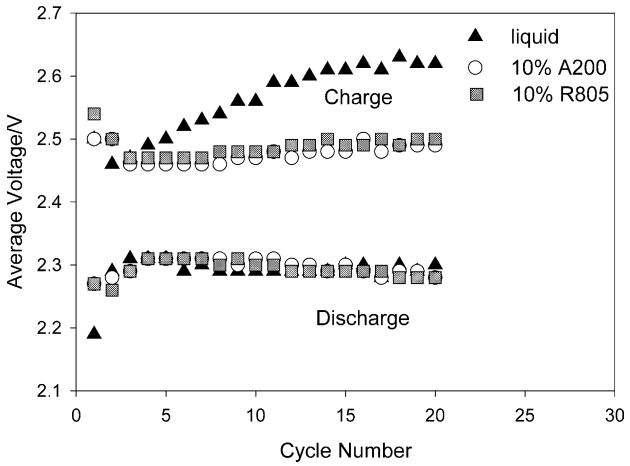

Fig. 9. Average charge–discharge voltage of Li/V_6O_{13} cells with different electrolytes at each cycle; the cycle conditions are those in Fig. 6.

The average charge–discharge voltage $\overline{V}_{C/D}$ is calculated by:

$$\overline{V}_{C/D} = \frac{\int_{C/D} V\,dt}{\int_{C/D} dt} = \frac{\int_{C/D} IV\,dt}{\int_{C/D} I\,dt} = \frac{\text{Energy}_{C/D}}{\text{Capacity}_{C/D}} \quad (3)$$

For liquid electrolyte, the average discharge voltage is approximately cycle-number independent at 2.3 V but the charge voltage increases from 2.5 to 2.6 V over 20 cycles. In contrast, for both composite electrolytes the discharge and charge voltages remain constant upon cycling at about 2.3 and 2.5 V, respectively. The 0.2 V difference between charge and discharge average voltage for both composite electrolytes can be attributed to the more stable interface between the composite electrolytes and electrodes. In fact, the difference of average charge and discharge voltage is reflected in the energy efficiency upon cycling, as seen in Equation 3.

The cycling efficiency indicates the extent of process reversibility. For lithium metal rechargeable cells, a coulombic efficiency of 99% [9] is reported to be acceptable. Fig. 10 reports the average coulombic and energy efficiency for the initial 20 cycles of Li/V_6O_{13} cells with the different electrolytes. While all coulombic efficiencies are high at about 99% (liquid electrolyte: 98.8%; 10% A200: 99.1%; and, 10% R805: 98.9%), the standard deviations δ over the 20 cycles for the coloumbic efficiency are in the sequence liquid electrolyte ($\delta = 2.3\%$) > 10% R805 ($\delta = 0.84\%$) > 10% A200 ($\delta = 0.60\%$). For the average energy efficiency, the order is 10% A200 (91.8%) > 10% R805 (90.2%) > liquid electrolyte (88.4%), and the standard deviations over the 20 cycles for the energy efficiency are in the order: liquid electrolyte ($\delta = 3.4\%$) > 10% R805 ($\delta = 1.4\%$) > 10% A200 ($\delta = 1.2\%$). These results show the reversibility and stability for the Li/V_6O_{13} cells with the electrolytes were in the sequence of 10% A200 > 10% R805 > liquid electrolyte.

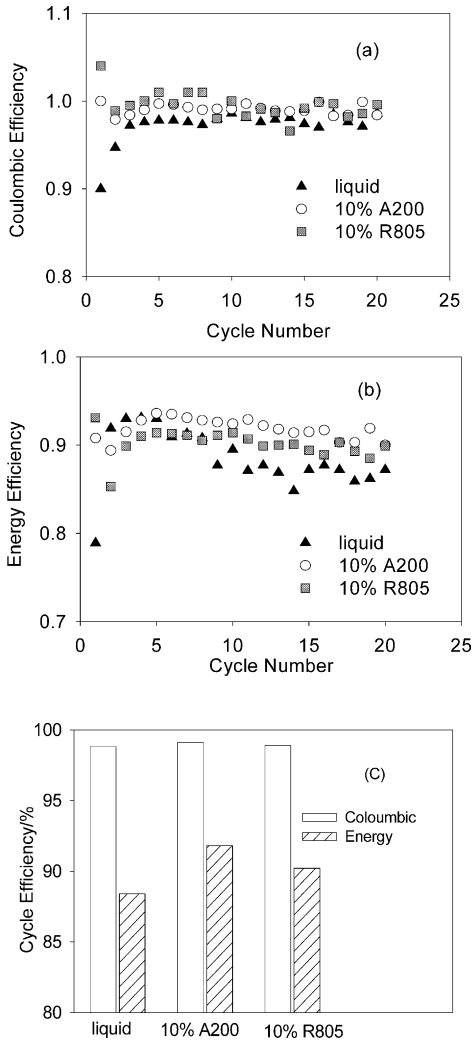

Fig. 10. Electrochemical efficiencies of Li/V_6O_{13} cells during first 20 cycles with different electrolytes. (a) Coulombic efficiency; (b) energy efficiency, (c) average efficiency during first 20 cycles, the cycle conditions as Fig. 6.

3.3. Effect of fumed silicas

The addition of fumed silicas to the PEGdm liquid electrolyte forms the composite gel electrolyte due to the self-assembly of the particulates and formation of three-dimensional continuous networks. The composite gel electrolyte exhibits desirable mechanical properties characteristic of solids, while they have the processability of liquid [1]. Adding fumed silica effectively suppresses the lithium dendrite growth and significantly improves the cycle performance and electrochemical efficiency. Although the improvements may be related to the trapping of trace impurities by the fumed silica, which has been ascribed to ceramic fillers as a mechan-

ism for improved behavior in high-molecular weight PEO [25], the most important effect should be ascribed to the stable and conductive interface between the electrodes and the electrolytes due to the rigidity and immobility of the composite gel electrolytes.

3.4. Effect of different surface groups

According to earlier work from our laboratory [1–3], ionic conductivity is essentially independent of the type of surface group present on the silica and decreases only slightly on addition of the fumed silicas. This is readily understood if one assumes that the liquid phase provides the ion-transport channel in the composite system. Although adding fumed silicas improves the electrochemical performance, the different surface groups on the fumed silicas have an effect on this improvement. The cell voltage and interfacial resistance for Li/Li cells with A200 are less than those with R805; the full-cell cycle performance and electrochemical efficiency with A200 are better than those with R805. If considering that there is inevitably residual moisture, the A200 fumed silicas having 100% hydrophilic silanol surface group is expected to exhibit better electrochemical performance than the R805 having 48% hydrophobic octyl surface group. Ideally, if we could design the surface group on fumed silicas to achieve high affinity with anions and solvents yet is repellent to lithium ions, the electrochemical performance of this gel electrolytes should be further improved. These studies are presently underway in our laboratory.

4. Conclusions

The electrochemical performance of a composite gel electrolyte at room temperature (22 °C) is discussed. Adding 10% fumed silicas A200 and R805 into the liquid electrolyte, which is composed of PEGdm+LiTFSI, forms a composite gel electrolyte as a direct consequence of the self-assembly of fumed silicas to establish a three-dimensional continuous network. The composites exhibit desirable mechanical properties characteristic of solids (elastic modulus $G' > 10^5$ Pa) and good conductivity rivaling liquid electrolyte (about 10^{-3} S cm^{-1} at room temperature).

The results from study of Li/electrolyte/Li cells reveal that the composite gel electrolytes effectively suppress lithium dendrite growth and have lower interfacial resistance compared with liquid electrolytes. The mechanism for inhibiting lithium dendrite is ascribed to the mechanical elastic characteristic of the composite system leading to the immobility of the electrolyte.

The performance of Li/electrolyte/V_6O_{13} cells is evaluated at C/15 (C as 417 mA h g^{-1}) with a voltage range from 1.8 to 3.0 V at room temperature (22 °C). The cycle performance and electrochemical efficiency for composite electrolytes is significantly superior to those for liquid electrolyte, which is attributed to the more stable and less resistive interface due to the immobility of the composite gel electrolytes. Since the composite electrolytes affect a stable and conductive interface between electrodes and electrolyte, the electrochemical performance of the cell improves considerably.

The effect of different surface groups on fumed silicas is discussed. If considering there is residual moisture in cells, it is readily understood that the fumed silicas having hydrophilic surface group, such as A200, behave better than those having a hydrophobic surface group, such as R805.

Acknowledgements

The authors gratefully acknowledge funding from the BATT program, Lawrence Berkeley Laboratory, US Department of Energy, and the DOE Office of Basic Energy Sciences.

References

[1] J. Fan, P.S. Fedkiw, J. Electrochem. Soc. 144 (1997) 399.
[2] J. Fan, S.R. Raghavan, X.Y. Yu, S.A. Khan, P.S. Fedkiw, J. Hou, G.L. Baker, Solid State Ionics 111 (1998) 117.
[3] H.J. Walls, J. Zhou, J.A. Yerian, P.S. Fedkiw, S.A. Khan, M.K. Stowe, G.L. Baker, J. Power Sources 89 (2000) 156.
[4] J. Hou, G.L. Baker, Chem. Mater. 10 (1998) 3311.
[5] R.J. Brodd, W. Huang, J.R. Akridge, Macromol. Symp. 159 (2000) 229.
[6] G. Feuillade, P. Perche, J. Appl. Electrochem. 5 (1975) 63.
[7] K. Murata, S. Izuchi, Y. Yoshihisa, Electrochim. Acta 45 (2000) 1501.
[8] C. Capiglia, Y. Saito, H. Yamamoto, H. Kageyama, P. Mustarelli, Electrochim. Acta 45 (2001) 1341.
[9] X. Wang, E. Yasukawa, S. Mori, J. Electrochem. Soc. 146 (1999) 3992.
[10] G. Michael, H. Ferch, Basic Characteristics of Aerosil, Degussa Technical Bulletin Pigment No. 11, 1998.
[11] S.R. Raghavan, H.J. Walls, S.A. Khan, Langmuir 16 (2000) 7920.
[12] S.R. Raghavan, J. Hou, G.L. Barker, S.A. Khan, Langmuir 16 (2000) 1066.
[13] K.E. Thomas, S.E. Sloop, J.B. Kerr, J. Newman, J. Power Sources 89 (2000) 132.
[14] J.N. Chazalviel, Phys. Rev. A 42 (1990) 7335.
[15] M. Rosso, T. Gobron, C. Brissot, J.N. Chazalviel, S. Lascaud, J. Power Sources 97–98 (2000) 804.
[16] T. Osaka, T. Homma, T. Momma, H. Yarimizu, J. Electroanal. Chem. 421 (1997) 153.
[17] T. Tatsuma, M. Taguchi, M. Iwaku, T. Sotomura, N. Oyama, J. Electroanal. Chem. 472 (1999) 142.
[18] T. Tatsuma, M. Taguchi, N. Oyama, Electrochim. Acta 46 (2001) 1201.
[19] D. Fauteux, Solid State Ionics 17 (1985) 133.
[20] W.J. Macklin, R.J. Neat, S.S. Sandhu, Electrochim. Acta 37 (1992) 1715.

[21] K. West, B. Zachau-Christiansen, T. Jacobsen, Electrochim. Acta 28 (1983) 1829.
[22] A.H. Thompson, J. Electrochem. Soc. 126 (1979) 608.
[23] Y. Xia, K. Tatsumi, T. Fujiida, P.P. Prosini, T. Sakai, J. Electrochem. Soc. 147 (2000) 2050.
[24] J. Barker, E.S. Saidi, M.Y. Saidi, Electrochim. Acta 40 (1995) 949.
[25] G.B. Appetecchi, F. Crose, M. Mastragostino, F. Ronci, B. Scrosati, F. Soavi, A. Zanelli, F. Alessandrini, P.P. Prosini, J. Electrochem. Soc. 145 (1998) 4126.